HHS Public Access

Author manuscript

*Cancer Immunol Res*. Author manuscript; available in PMC 2021 June 28.

Published in final edited form as:

*Cancer Immunol Res*. 2019 March ; 7(3): 401–413. doi:10.1158/2326-6066.CIR-18-0546.

# Host immunity following near-infrared photoimmunotherapy is enhanced with PD-1 checkpoint blockade to eradicate established antigenic tumors

**Tadanobu Nagaya**[1], **Jay Friedman**[2], **Yasuhiro Maruoka**[1], **Fusa Ogata**[1], **Shuhei Okuyama**[1], **Paul E. Clavijo**[2], **Peter L. Choyke**[1], **Clint Allen**[2,*], **Hisataka Kobayashi**[1,*]

[1]Molecular Imaging Program, Center for Cancer Research, National Cancer Institute, National Institutes of Health, Bethesda, Maryland, 20892, United States of America

[2]Translational Tumor Immunology Program, National Institute on Deafness and Other Communication Disorders, National Institutes of Health, Bethesda, Maryland, 20892, United States of America

## Abstract

Near-infrared photoimmunotherapy (NIR-PIT) induces immunogenic cell death, but has mostly failed to induce durable antitumor responses in syngenic tumor mouse models. We hypothesized that adaptive immune resistance could be limiting durable responses after treatmemt with NIR-PIT. We investigated the effects of combining NIR-PIT targeting cell surface CD44 and PD-1 blockade in multiple syngeneic tumor models. In two of three models, NIR-PIT monotherapy halted tumor growth, enhanced dendritic cell tumor infiltration, and induced *de novo* tumor antigen-specific T-cell responses absent at baseline. The addition of PD-1 blockade reversed adaptive immune resistance, resulting in both enhanced pre-existing tumor antigen-specific T-cell responses and enhanced *de novo* T-cell responses induced by NIR-PIT. Enhanced immune responses correlated with shared tumor antigen expression, suggesting that antigenicity is a major determinant of response to combination NIR-PIT and PD-1 blockade. Combination treatment induced complete rejection of MC38 tumors treated with NIR-PIT, as well as untreated, distant tumors. Accordingly, tumor antigen-specific T-cell responses were measured in both treated and untreated tumors, validating the development of systemic antitumor immunity. Mice that cleared tumors resisted subsequent tumor challenge, indicating the presence of systemic immune memory.

[*]Corresponding senior authors: Clint Allen, M.D., National Institutes of Health, Building 10, Room 7N240C, 10 Center Drive Bethesda, MD 20892, Ph: 301-827-5620; Fax: 301-402-1140; clint.allen@nih.gov and Hisataka Kobayashi, M.D., Ph.D., National Institutes of Health, Building 10, Room B3B69, MSC 1088, 10 Center Drive, Bethesda, MD 20892, Ph: 240-858-3069; Fax: 240-541-4527; kobayash@mail.nih.gov.

Authors' Contributions

**Conception and design:** T. Nagaya, C. Allen, P.L. Choyke, H. Kobayashi

**Development of methodology:** T. Nagaya, J. Friedman, C. Allen, H. Kobayashi

**Acquisition of data (provided animals, acquired and managed patients, provided facilities, etc.):** T. Nagaya, J. Friedman, Y. Maruoka, F. Ogata, S. Okuyama, P.E. Clavijo, C. Allen, H. Kobayashi

**Analysis and interpretation of data (e.g., statistical analysis, biostatistics, computational analysis):** T. Nagaya, J. Friedman, Y. Maruoka, F. Ogata, S. Okuyama, P.E. Clavijo, C. Allen, H. Kobayashi **Writing, review, and/or revision of the manuscript:** T. Nagaya, C. Allen, P.L. Choyke, H. Kobayashi

**Administrative, technical, or material support (i.e., reporting or organizing data, constructing databases):** T. Nagaya, J. Friedman, Y. Maruoka, F. Ogata, S. Okuyama, P.E. Clavijo, C. Allen, H. Kobayashi **Study supervision:** C. Allen, H. Kobayashi

Disclosure of Potential Conflicts of Interest

No potential conflicts of interest were disclosed.

Cumulatively these results demonstrate reversal of adaptive immune resistance following induction of innate and adaptive immunity by NIR-PIT, resulting in high rates of tumor rejection and/or significant tumor growth control in antigenic syngeneic models of cancer.

**Keywords**

photoimmunotherapy; antigenicity; adative immune resistance; immune checkpoint inhibition; polyclonal T cell response

## INTRODUCTION

Near-infrared photoimmunotherapy (NIR-PIT) is a newly developed cancer treatment that employs a targeted monoclonal antibody–photo-absorber conjugate (1). Following antibody localization of the antibody–photo-absorber conjugate to a tumor cell surface antigen, NIR light is used to induce selective cytolysis. NIR-PIT targeting EGFR with a cetuximab-antibody–photo-absorber conjugate has shown promising results in phase II clinical evaluation for the treatment of recurrent head and neck squamous cell carcinoma (NCT02422979) and has received breakthrough therapy designation by the Food and Drug Administration. Extensive pre-clinical evidence demonstrates that NIR-PIT is effective at inducing tumor cell lysis using a number of different antibody–antibody–photo-absorber conjugates (2–6).

NIR-PIT induces rapid, necrotic cell death that yields innate immune ligands that activate dendritic cells (DCs) (7), consistent with immunogenic cell death (ICD) (8). Yet, NIR-PIT treatment of syngeneic tumors in wild-type mice has mostly failed to induce durable regression of established tumors (2), suggesting the presence of one or more mechanisms of resistance to formation of meaningful antitumor immunity. Expression of programmed death ligand-1 (PD-L1), in response to local immune activation and interferon (IFN) production, may bind the programmed death receptor (PD-1) on T lymphocytes and inhibit T-cell receptor signaling, proliferation, and mobility in a process known as adaptive immune resistance (9–11). Immune checkpoint blockade (ICB) with anti–PD-1/anti–PD-L1 induces objective and sometimes durable antitumor immune responses, but only in a subset (15–20%) of patients with recurrent/metastatic cancer (12, 13). Given that PD-1 inhibition re-activates T cells being inhibited by PD-1 signaling and that response to PD-1 blockade correlates with the presence of inducible adaptive immune responses (10, 14), anti-cancer treatments that enhance baseline adaptive immunity may enhance responses to PD-1 ICB.

In this study, we hypothesized that NIR-PIT could induce antitumor immunity being restricted by the PD-1/PD-L1 signaling axis and that PD-1 ICB could reverse innate immune resistance to induce durable, effective antitumor immune responses. Using a CD44-targeting antibody–photo-absorber conjugate, we demonstrated the ability of PD-1 ICB to significantly enhance antigen-specific antitumor immunity induced by NIR-PIT in multiple models of cancer. Combination treatment resulted in significant growth control or rejection of established colon (MC38) and lung (LLC) tumors. Assessment of antigen-specific tumor-infiltrating lymphocyte (TIL) responses against shared tumor-associated antigens revealed enhancement of pre-existing and NIR-PIT–induced antigen-specific responses in tumors.

Efficacy of the combination treatment between different syngeneic models correlated with NIR-PIT surface target antigen expression, baseline tumor-associated antigen (TAA) expression, and induction of DC tumor infiltration. Taken together, this dataset provides insight into mechanisms of resistance following NIR-PIT and provides a rationale for the clinical combination of NIR-PIT and ICB.

## Materials and Methods

### Reagents

Water soluble, silica-phthalocyanine derivative, IRDye 700DX NHS ester (IR700) was obtained from LI-COR Biosciences (Lincoln, NE, USA). Anti-mouse/human CD44-specific mAb (clone IM7) and an anti-mouse PD-1 (CD279) specific mAb (clone RMP1–14) were purchased from BioXCell (West Lebanon, NH, USA). All other chemicals were of reagent grade.

### Synthesis of IR700-conjugated anti-CD44

Anti-CD44 (1.0 mg, 6.7 nmol) was incubated with IR700 NHS ester (65.1 μg, 33.3 nmol) in 0.1 M $Na_2HPO_4$ (pH 8.6) at room temperature for 1 hour and purified with a Sephadex G25 column (PD-10; GE Healthcare, Piscataway, NJ, USA). Protein concentration was determined with Coomassie Plus protein assay kit (Thermo Fisher Scientific Inc, Rockford, IL, USA) by measuring the absorption at 595 nm with UV-Vis (8453 Value System; Agilent Technologies, Santa Clara, CA, USA). IR700 concentration was measured by absorption at 689 nm to confirm the number of fluorophore molecules per monoclonal antibody (mAb). CD44-IR700 conjugate synthesis was controlled so that an average of two IR700 molecules were bound to each CD44 antibody. Fluorescence at 700 nM and the molecular weight of CD44-IR700 conjugates (~150 kD) was verified using sodium dodecyl sulfate-polyacrylamide (4–20% gradient) gel electrophoresis (SDS-PAGE).

### Cell lines and culture

MC38 (colon cancer, kind gift from Claudia Palena, NCI) cells stably expressing luciferase (MC38-luc, generated via stable transduction with RediFect Red-Fluc lentivirus from PerkinElmer per manufacturer recommendations), LLC (Lewis lung carcinoma, kind gift of James Hodge, NCI) cells, and MOC1 (murine oral carcinoma, kind gift from Ravindra Uppaluri, Washington University in St. Louis) cells were maintained in culture as previously described (15–17). Briefly, cells were cultured in IMDM/F12 (2:1) with 5% fetal calf serum, penicillin (50 U/mL) and streptomycin (50 μg/mL), 1% amphotericin, and EGF (5 ng/mL; Millipore). MOC1 cells were used from original stocks of exome-sequenced cells, otherwise, cell line authentication was performed via *in vitro* growth characteristics. Cells were maintained in culture for no more than 30 passages and routinely tested negative for mycoplasma and murine-associated pathogens.

### *In vitro* NIR-PIT

MC38-luc, LLC, or MOC1 cells ($2 \times 10^5$) were seeded into 12-well plates, incubated for 24 hours, and then exposed to media containing CD44-IR700 (10 μg/mL) for 6 hours at 37°C. Cells were irradiated with a red light-emitting diode (LED, 690 ± 20 nm wavelength,

L690-66-60; Marubeni America Co., Santa Clara, CA, USA) at a power density of 50 mW/cm$^2$. Cells were harvested with a cell scraper, stained with propidium iodide (PI, 2 μg/mL) at room temperature for 30 minutes, and then assessed for PI positivity on a BD FACS Calibur (BD Biosciences) using CellQuest software.

## Animal and tumor models

All *in vivo* procedures were approved by the local Animal Care and Use Committee. Six to eight-week-old female wild-type C57BL/6 mice (strain #000664) were purchased from Jackson Laboratory (Sacramento, CA, USA). Mice were shaved at sites of subcutaneous tumor transplantation prior to injection. Tumors were established via subcutaneous injection of $6 \times 10^6$ cells in the caudal flank for each model. In some experiments, multiple subcutaneous MC38 tumors were established (contralateral caudal flank and bilateral cranial flanks). Established tumors were treated at volumes of approximately 50 mm$^3$ (4 to 5 mm in diameter; day 4 for MC38-luc and LLC tumors; day 18 for MOC1 tumors).

For NIR-PIT treatments and fluorescence/bioluminescence imaging (BLI), mice were anesthetized with inhaled 3–5% isoflurane and/or via intraperitoneal injection of 1 mg of sodium pentobarbital (Nembutal Sodium Solution, Ovation Pharmaceuticals Inc., Deerfield, IL, USA). CD44-IR700 was administered via IV (tail-vein) injection and NIR light was administered at 50 J/cm$^2$ on day 5 and 100 J/cm$^2$ on day 6. Previous results from our laboratory have demonstrated that two NIR light doses kill up to 80% of target-expressing cells (1, 2). For mice bearing multiple tumors, tumors not exposed to NIR were shielded from NIR light exposure with aluminum foil. Anti–PD-1 (clone RMP1–14, BioXCell, 100–200 μg/injection as indicated in figures) or isotype control (clone 2A3, BioXCell) was administered via intraperitoneal injection. Tumor volumes were based on three times weekly caliper measurements (tumor volume = length × width$^2$ × 0.5).

In some MC38 experiments, mice cleared of tumors after combination NIR-PIT and anti–PD-1 treatment were challenged via subcutaneous injection of MC38 ($6 \times 10^6$) cells in the contralateral flank. Tumor volume and animal weight was measured three times a week for MC38-luc and LLC tumors and two times a week for MOC1 tumors until the tumor volume reached 2000 mm$^3$, whereupon the mice were euthanized with inhalation of carbon dioxide gas. For all immune correlative experiments, mice were euthanized via awake cervical dislocation.

## Fluorescence imaging

*In vitro*, MC38-luc, LLC, or MOC1 cells ($1 \times 10^4$) were seeded on cover-glass-bottom dishes, incubated for 24 hours, and then exposed to CD44-IR700 (clone IM7, 10 μg/mL) for 6 hours at 37°C. Cells were then analyzed via fluorescence microscopy (BX61; Olympus America, Inc., Melville, NY, USA) using a 590–650 nm excitation filter and a 665–740 nm band pass emission filter. Transmitted light differential interference contrast (DIC) images were also acquired.

*In vivo*, IR700 fluorescence and white light images were obtained using a Pearl Imager (700 nm fluorescence channel) and analyzed using Pearl Cam Software (LICOR Biosciences, Lincoln, NE). Regions of interest (ROIs) within the tumor (n=10) were compared to adjacent

non-tumor regions as background (left dorsum). Average fluorescence intensity of each ROI was calculated.

### Bioluminescence imaging (BLI)

*In vitro*, MC38-luc cells were seeded into 12-well plates ($2 \times 10^5$ cells/well) or a 10 cm dish ($2 \times 10^7$ cells), incubated for 24 hours, then exposed to CD44-IR700 (10 μg/mL) for 6 hours at 37˚C. Cells were treated with LED or NIR laser light (690 ± 5 nm, BWF5–690-8–600-0.37; B&W TEK INC., Newark, DE, USA) in phenol red-free culture medium. For luciferase activity, cells were exposed to D-luciferin (150 μg/mL; Gold Biotechnology, St. Louis, MO, USA) 1 hour after NIR-PIT treatment, and luciferase activity (photons/min) was obtained on a BLI system (Photon Imager; Biospace Lab, Paris, France) using M3 Vision Software (Biospace Lab). *In vivo*, D-luciferin (15 mg/mL, 200 μL) was injected intraperitoneally, and the mice were analyzed on a BLI system (Photon Imager) for luciferase activity (photons/min/$cm^2$). ROIs were set to include the entire tumor with the adjacent non-tumor region as background.

### Histological analysis

Tumors (day 10 for MC38-luc and LLC tumors, day 24 for MOC1 tumors) were excised, formalin-fixed and paraffin embedded, and sectioned at 10 μm. Following standard H&E staining, brightlight photomicrographs were obtained on an Olympus BX61 microscope.

### Immunofluorescence

Formalin-fixed paraffin-embedded sections were stained as described (18). Briefly, sections were deparaffinized in an ethanol gradient, then blocked in separate incubations with bloxall (Vector Laboratories), 2.5% normal goat serum (Vector Laboratories), and Renaissance antibody diluent (Biocare Medical). A primary antibody targeting CD4 (Invitrogen, clone 4SM95, 1:75 dilution) in Renaissance antibody diluent was added for 45 minutes on an orbital shaker. Slides were washed five times then stained with an anti-rat secondary antibody (Vector Laboratories). Following four more washes, slides were stained with TSA-conjugated Opal650 (Perkin Elmer, 1:150 dilution) in Amplification Plus buffer (Perkin Elmer). Slides were washed four times with 1X TBS-T. Slides were washed, exposed to antigen stripping buffer (0.1 M glycine pH10 + 0.5% tween 20), and re-blocked as above. A primary antibody targeting CD8 (Invitrogen, clone 4SM15, 1:75 dilution) in Reinassance antibody diluent was added for 45 minutes. Anti-rat secondary antibody (Vector Laboratories) was added as above. Following four more washes, slides were stained with TSA conjugated Opal520 (Perkin Elmer, 1:150 dilution) in Amplification Plus buffer (Perkin Elmer). Nuclei counter-staining was achieved with Spectral DAPI (Perkin Elmer, 1:500). Slides were rinsed once with $ddH_2O$, cover-slipped with Vectashield hard mount (Vector Laboratories), and sealed with clear nail polish (Revlon).

### Flow cytometry

*In vitro*, MC38-luc, LLC, or MOC1 cells ($2 \times 10^5$) were seeded into 12-well plates and incubated for 24 hours. The cells were then exposed to media containing CD44-IR700 (10 μg/mL) for 6 hours at 37°C. Cells were harvested and analyzed on a BD FACS Calibur (BD

Biosciences) using CellQuest software. To validate specific binding of CD44-IR700, cells were incubated with excess unconjugated CD44 antibody (clone IM7, BioXCell, 100 μg) prior to incubation with CD44-IR700.

*In vivo*, tumors were harvested (day 10 for MC38-luc and LLC tumors, day 24 for MOC1 tumors) and immediately digested as previously described (19). Briefly, minced tumors were digested using the mouse tumor dissociation kit (Miltenyi) and the GentleMACS dissociator (Miltenyi). Digests were filtered and suspended in cold 1xPBS in 1% BSA for staining. Following FcγR (CD16/32) blocking (clone 93, 1 μg/mL, 10 min on ice), single cell suspensions were stained with fluorophore-conjugated primary antibodies: anti-mouse CD45.2 (clone 104), CD3 (clone 145–2C11), CD8 (clone 53–6.7), CD4 (clone GK1.5), PD-1 (clone 29F.1A12), CD11c (clone N418), F4/80 (clone BM8), CD11b (clone M1/70), Ly-6C (clone HK1.4), Ly-6G (clone 1A8), I-A/I-E (clone M5/114.15.2), PD-L1 (clone 10F.9G2), CD25 (clone PC61.5.3), CTLA-4 (clone UC10–4B9), CD31 (clone 390), PDGFR (clone APA5), and CD44 (clone IM7) (all from Biolegend). Cell were incubated with primary antibodies for one hour in a 1% BSA/1x PBS buffer. Suspensions were washed, stained with a viability marker (7AAD or zombie aqua; Biolegend) and analyzed on a BD Canto using BD FACS Diva software. Isotype controls and "fluorescence minus one" controls were used to validate staining specificity. FoxP3$^+$ regulatory CD4$^+$ T-lymphocytes ($T_{regs}$) were stained using the Mouse Regulatory T Cell Staining Kit #1 (eBioscience) and associated fix and permeabilization buffers per the manufacturer's protocol. Post-acquisition analysis was performed with FlowJo vX10.0.7r2.

## Antigen-specific TIL reactivity

Minced fragments of fresh MC38, LLC, or MOC1 tumors were incubated in RPMI 1640 media supplemented with glutamine (2 nM), HEPES (25 mM), 1 mM sodium pyruvate, 10 μM β-mercaptoethanol, 5% FBS, and recombinant murine IL2 (100 U/mL; Biolegend) for 72 hours. Untouched TILs were enriched to >95% purity with negative magnetic sorting (Pan T Cell Isolation Kit II, AutoMACSpro, Miltenyi Biotec). Antigen-presenting cells (APCs; whole splenocytes from naïve, WT B6 mice from Taconic, irradiated with 50 Gy) were pulsed for one hour with peptides of interest: class I-restricted antigen $p15E_{604–611}$ (H-2K$^b$-restricted KSPWFTTL) (20), survivin/$Birc5_{57–64}$ (H-2K$^b$-restricted QCFFCFKEL) (21), $Twist_{125–133}$ (H-2D$^b$-restricted TQSLNEAFA), and $Trp53_{232–240}$ (H-2D$^b$-restricted KYMCNSSCM) (22). Peptides were synthesized by Peptide2.0. Antigen-pulsed APCs and TILs were co-incubated for 24 hours at a 3:1 APC:TIL ratio. Supernatants (50 μL) were analyzed for IFNγ production by ELISA (Mouse IFNγ Quantikine ELISA kit, R&D) per manufacturer recommendations. TILs alone, APCs alone, and peptide stimulations with $ovalbumin_{257–264}$ (H-2K$^b$-restricted SIINFEKL) and VSV-$N_{52–59}$ (H-2D$^b$-restricted RGYVYQGL) were used as controls.

## Quantitative RT-PCR

RNA from whole MC38, LLC, or MOC1 tumor lysates generated via Tissue Lyser II mechaniscal dissociation was purified using the RNEasy Mini Kit (Qiagen) per the manufacturer's protocol. RNA purity and quantity was assessed on a Nanodrop Spectrophotometer based on basorbance at 260/280 and 260/230. cDNA was synthesized

utilizing a high capacity cDNA reverse transcription kit with RNase inhibitor (Applied Biosystems) beginning with 2 μg or RNA template. A Taqman Universal PCR master mix was used to assess the relative expression ($\Delta\Delta CT^2$) of target genes compared to *Gapdh* on a Viia7 qPCR analyzer (Applied Biosystems) in technical triplicates. Custom primers were designed to flank nucleotide regions encoding the MHC class I-restricted epitopes for each tumor-associated antigen (Supplementary Table S1).

### Statistical analysis

Data are expressed as means ± SEM from a minimum of five experiments, unless otherwise indicated. Statistical analyses were carried out using GraphPad Prism version 7 (GraphPad Software, La Jolla, CA, USA). Student's t test was used to compare the treatment effects with that of control *in vitro*. To compare tumor growth in a re-inoculated tumor model of MC38-luc, the Mann Whitney test was used. For multiple comparisons, a one-way analysis of variance (ANOVA) followed by the Tukey's test was used. The cumulative probability of survival based on volume (2000 $mm^3$) were estimated in each group with a Kaplan-Meier survival curve analysis, and the results were compared with use of the log-rank test. A *p*-value of $< 0.05$ was considered statistically significant.

## RESULTS

### Confirmation of CD44 expression as a target for NIR-PIT

Using gel electrophoresis, CD44-IR700 conjugates demonstrated no appreciable aggregates, having a similar molecular weight to CD44 mAb alone. Conjugates demonstrated strong fluorescent intensity (Fig. 1A) and peak absorbance around 690 nm (Fig. 1B) as expected for IR700. Flow cytometric and fluorescent microscopic analysis revealed a high fluorescent signal in MC38-luc (Fig. 1C–D), LLC (Supplementary Fig. S1A–B), and MOC1 (Supplementary Fig. S2A–B) cells after exposure to CD44-IR700. This signal was completely reversed in the presence of excess unconjugated CD44 mAb, verifying binding specificity. NIR light exposure of tumor cells exposed to CD44-IR700 induced immediate cellular swelling, bleb formation, and rupture of vesicles indicative of necrotic cell death in all three cell lines (Supplementary Videos S1–S3). These morphologic changes were observed within 15 minutes of NIR exposure (Fig. 1D, Supplementary Figs. S1B and S2B). Bioluminescence imaging demonstrated decreased luciferase activity in a light-dose dependent manner (Fig. 1E–F) in MC38-luc cells. Based on incorporation of propidium iodine, NIR induced cell death in a light-dose dependent manner in MC38-luc (Fig. 1G), LLC (Supplementary Fig. S1C), and MOC1 (Supplementary Fig. S2C) cells exposed to CD44-IR700. NIR nor CD44-IR700 alone did not induce significant alterations in cell viability. These data validated that NIR-PIT targeting CD44 induced specific cell death in MC38-luc, LLC, and MOC1 cells *in vitro*.

### CD44 expression within MOC1, LLC, and MC38-luc tumor compartments

To verify target expression of CD44 *in vivo*, size matched MOC1 (day 24), LLC (day 10), and MC38 (day 10) tumors were assessed for CD44 expression within different tumor compartments via flow cytometry (Supplementary Fig. S3A). Significant heterogeneity in tumor and stromal cell-specific CD44 expression was observed, with LLC and MC38-luc

tumor cells expressing significantly greater CD44 compared to MOC1. Expression of CD44 on immune cell subsets was more homogeneous between MOC1, LLC, and MC38-luc tumors and was greater than CD44 expression on tumor and stromal cells on a cell-by-cell basis as measured by mean fluorescence intensity (MFI). Whole tumor accumulation of CD44-IR700 one day after injection, which is dependent upon multiple factors including target antigen expression and vascularity, was significantly greater in MC38-luc tumors ($p<0.001$) compared to LLC or MOC1 tumors (Supplementary Fig. S3B–C).

### *In vivo* effect of NIR-PIT and PD-1 mAb in mice bearing unilateral tumors

We previously demonstrated the antitumor effects of NIR-PIT targeting CD44 in syngeneic murine models of oral cancer (2) and that NIR-PIT treatment, in general, can lead to immunogenic cell death and promote antitumor inflammatory responses (7). Thus, we hypothesized that the addition of systemic PD-1 immune checkpoint blockade (ICB) to local, CD44-directed NIR-PIT would reverse adaptive immune resistance (10) and enhance antitumor responses. The NIR-PIT and PD-1 mAb treatment regimen and imaging protocol (Fig. 2A) for treatment of unilateral MC38-luc tumors (Fig. 2B) are depicted. Compared to control or PD-1 mAb alone groups, NIR-PIT resulted in a near-immediate decrease in tumor fluorescence signal, likely due to dispersion of IR700 from dying cells (Fig. 2C). Combination NIR-PIT and PD-1 mAb treatment resulted in dramatically decreased bioluminescence compared to control or single treatment groups (Fig. 2D–E). Histologic (H&E) analysis of treated tumors revealed extensive tumor necrosis and micro-hemorrhage in tumors treated with NIR-PIT, whereas groups treated with PD-1 mAb demonstrated greater leukocyte infiltration (Fig. 2F). Although primary tumor growth was inhibited following NIR-PIT or PD-1 mAb alone compared to control (Fig. 2G), combination treatment resulted in significant tumor control and complete rejection of established MC38-luc tumors in 9 of 13 (70%) mice and resulted in significantly prolonged survival (Fig. 2H). Neither skin necrosis nor systemic toxicity was observed within any treatment group.

Similar approaches were taken in mice bearing established unilateral LLC or MOC1 tumors using similar treatment regimens and imaging protocols (Supplementary Figs. S4A and S5A). Similar to MC38-luc tumors, treatment of LLC or MOC1 tumors with NIR-PIT resulted in near-immediate loss of IR700 fluorescent signal (Supplementary Fig. S4B and S5B) indicating on-target effects. Treatment of LLC tumor-bearing mice with combination NIR-PIT and PD-1 mAb significantly enhanced primary tumor control (Supplementary Fig. S4C) and survival (Supplementary Fig. S4D) over control or either treatment alone, and resulted in rejection of 1 of 12 (8%) established tumors. Treatment of MOC1 tumor-bearing mice with combination NIR-PIT and PD-1 mAb induced rejection of 1 of 13 (8%) established tumors and resulted in statistically enhanced survival compared to control, but cumulative primary tumor growth following combination treatment was not enhanced over either treatment alone (Supplementary Fig. S5C–D). Taken together, these results demonstrated CD44 on-target effects of NIR-PIT in MC38-luc, LLC, and MOC1 tumor-bearing mice, with significant enhancement of primary tumor control and survival with the addition of PD-1 ICB in the MC38-luc and LLC models.

### Antigen-specific immunity is induced with NIR-PIT and enhanced by PD-1 ICB

Following completion of treatment, some MC38-luc tumors were processed into single-cell suspensions and assessed for infiltration of immune cells with flow cytometry. Tumors treated with NIR-PIT demonstrated significantly enhanced infiltration by $CD8^+$ and $CD4^+$ lymphocytes (Fig. 3A) that expressed greater PD-1. Mice treated with systemic PD-1 mAb demonstrated PD-1 target saturation, as very low levels of PD-1 were detectible on the surface of TILs from these tumors by flow cytometry after staining with the same antibody clone (RMP1–14). This enhanced $CD8^+$ and $CD4^+$ TIL infiltration was verified by multiplex immunofluorescence (IF). In control- or PD-1 mAb–treated tumors, few $CD8^+$ TILs nested along the tumor-stromal interface but did not infiltrate the tumor (Fig. 3B, left panels). Following NIR-PIT, more $CD8^+$ TILs infiltrated throughout the tumor, but many TILs were still arrested at the tumor-stromal interface. Infiltration into the tumor was significantly enhanced with the addition of PD-1 mAb (Fig. 3B, right panels). In additional experiments, TILs were extracted from control or treated MC38-luc tumors via IL2, and assessed for antigen-specific IFN$\gamma$ responses to multiple known H-$2K^b$ or H-$2K^d$-restricted TAAs (Fig. 3C). TILs from control tumors demonstrated measurable responses to H-$2K^b$-restricted $p15E_{604–611}$ (KSPWFTTL) but lacked responses to other antigens. PD-1 mAb treatment enhanced the baseline $p15E_{604–611}$ responses but did not induce responses against other antigens. NIR-PIT treatment induced *de novo* responses that were absent at baseline to H-$2K^b$-restricted survivin/$Birc5_{57–64}$ (QCFFCFKEL) and H-$2D^b$-restricted $Trp53_{232–240}$ (KYMCNSSCM) and enhanced baseline responses to $p15E_{604–611}$. Treatment with PD-1 mAb enhanced these NIR-PIT induced or enhanced antigen-specific responses. NIR-PIT also enhanced tumor infiltration of MHC class $II^+$ dendritic cells (DCs) and $F4/80^+$ macrophages polarized to express greater MHC class II (Fig. 3D). Immunosuppressive neutrophilic-myeloid (PMN-myeloid) and regulatory $CD4^+$ T-lymphocytes ($T_{regs}$) were variably altered by combination treatment (Fig. 3E). MC38-luc tumor cell–specific PD-L1 expression was verified but did not change with treatment, whereas infiltrating immune cell PD-L1 was significantly greater than tumor cell expression and increased with combination treatment (Fig. 3F).

Similar immune correlative experiments were carried out in LLC and MOC1 tumors. LLC tumors treated with PD-1 mAb and NIR-PIT alone or in combination demonstrated enhanced TIL infiltration (Supplementary Fig. S6A). Antigen-specific LLC TILs demonstrated measurable baseline responses to $p15E_{604–611}$ and H-$2D^b$-restricted $Twist_{125–133}$ (TQSLNEAFA). Similar to MC38-luc tumors, NIR-PIT treatment induced responses to survivin/$Birc5_{57–64}$. Responses to Birc5 and Twist but not p15E were enhanced with PD-1 mAb treatment (Supplementary Fig. S6B). NIR-PIT treatment of LLC tumors enhanced infiltration of MHC class $II^+$ DCs and MHC class II expression on macrophages (Supplementary Fig. S6C). PMN-myeloid cells and $T_{regs}$ were variably altered following treatments (Supplementary Fig. S6D), and LLC tumor and immune cell-specific PD-L1 expression was enhanced with treatment (Supplementary Fig. S6E). In contrast to MC38-luc or LLC tumors, MOC1 tumors treated with NIR-PIT demonstrated few immune correlative alterations. $CD8^+$ and $CD4^+$ TIL infiltration was enhanced with PD-1 mAb but not NIR-PIT (Supplementary Fig. S7A). Baseline TIL antigen-specific responses to $p15E_{604–611}$ were enhanced with systemic PD-1 mAb treatment, but responses to other shared tumor antigens

were not induced with NIR-PIT treatment (Supplementary Fig. S7B). Assessment of MOC1 tumor infiltration of MHC class $II^+$ DCs and macrophages suggested a lack of myeloid cell priming and activation in this model. No significant changes were observed in infiltration of PMN-myeloid cells or $T_{regs}$ or MOC1 tumor or immune cell-specific PD-L1 expression (Supplementary Fig. S7C–D).

To investigate possible explanations for the lack of TIL responses against tumor-associated antigens in MOC1, we measured relative expression of each antigen within MC38-luc, LLC, and MOC1 cells. Using primers designed to flank the MHC class I-restricted epitope coding region, PCR results indicated low expression of *Birc5*, *Twist1*, and *Trp53* gene transcripts in MOC1 relative to MC38-luc and LLC (Supplementary Fig. S8). Greater antigen expression generally correlated with baseline TIL responses. Higher relative *Trp53* expression in MC38-luc cells and *Twist1* expression in LLC cells correlated to enhanced TIL responses against the class I-restricted epitopes from these genes after combination NIR-PIT and PD-1 mAb treatment. Although correlative, these data suggest that enhanced TIL responses after treatment may be dependent on baseline tumor antigen expression. Taken together, these results indicated that NIR-PIT can induce *de novo*, polyclonal antigen-specific TIL responses against MHC class I-restricted tumor antigens in MC38-luc and LLC tumor-bearing mice, and that these responses can be enhanced with systemic PD-1 ICB.

## Combination NIR-PIT and PD-1 ICB induces an abscopal antitumor effect in mice

Given evidence of induction of tumor antigen-specific immunity following NIR-PIT in MC38-luc tumor-bearing mice, we next assessed whether local NIR-PIT combined with systemic PD-1 mAb could induce antitumor immunity in a separate, distant tumor not treated with NIR-PIT. Treatment and imaging regimens (Fig. 4A) were similar for mice bearing bilateral MC38-luc tumors as previously described, but only the right flank tumor was treated with NIR-PIT (Fig. 4B). NIR-PIT induced near-immediate loss of IR700 fluorescent signal in the treated tumor, whereas loss of IR700 signal intensity in the untreated tumor was delayed for several days (Fig. 4C). Conversely, bioluminescence of both right (treated with NIR-PIT) and left (untreated) MC38-luc tumors decreased concurrently after combination treatment (Fig. 4D–E). Histologic analysis of both right and left tumors revealed similar patterns of necrosis and micro-hemorrhage and increase leukocyte infiltration (Fig. 4F). Combination treatment resulted in significant primary tumor control and complete tumor rejection of both right and left tumors in 8 of 10 mice (80%; Fig. 4G), leading to enhanced survival compared to untreated mice (Fig. 4H).

## Induction of antigen-specific immunity in distant tumors not treated with NIR-PIT

Flow cytometric analysis of single-cell suspensions from both right (treated with NIR-PIT) and left (untreated) tumors revealed similar enhancement of $CD8^+$ and $CD4^+$ TIL accumulation (Fig. 5A). Assessment of antigen-specific reactivity demonstrated that TILs from both treated and untreated tumors reacted to the same MHC class I-restricted antigens (Fig. 5B), indicating the presence of systemic antigen-specific immunity. TIL responses were similar in magnitude to $p15E_{604–611}$ and survivin/$Birc5_{57–64}$, but responses to $Trp53_{232–240}$ were diminished in tumors not treated with NIR-PIT compared to treated. Increased MHC class $II^+$ DCs and macrophages (Fig. 5C), increased PMN-myeloid cells,

and decreased $T_{regs}$ (Fig. 5D) were observed in treated but not untreated tumors, suggesting these changes are a direct result of NIR-PIT and not a result of systemic antitumor immunity. MC38-luc infiltrating immune cell PD-L1 expression (Fig. 5E) was enhanced in both right (treated) and left (untreated) tumors in mice receiving combination treatment, indicating that immune cell PD-L1 expression may be independent of NIR-PIT. These results together demonstrated that combination NIR-PIT and PD-1 ICB can lead to the development of systemic tumor antigen-specific immunity capable of eliminating an established untreated tumor, but that enhanced innate immunity and alterations in immunosuppressive cell subsets appear to occur locally as a more direct effect of NIR-PIT.

## Combination NIR-PIT and PD-1 ICB leads to control of multiple distant tumors

We next investigated whether treatment of a single MC38-luc tumor could lead to rejection of multiple established distant tumors within an individual mouse. Similar treatments (Fig. 6A) were used to deliver NIR-PIT to one of four established MC38 tumors (Fig. 6B). NIR-PIT induced near-immediate loss of IR700 fluorescent signal in the single treated tumor, whereas resolution of IR700 signal intensity in the three untreated tumors was delayed for several days (Fig. 6C). Conversely, bioluminescence of both the single treated and three untreated MC38-luc tumors decreased concurrently after combination treatment (Fig. 6D–E). Histologic analysis revealed necrosis and increased leukocyte infiltration in all tumors from treated mice but not tumors from control mice (Fig. 6F). Systemic PD-1 mAb and treatment of a single MC38-luc tumor with NIR-PIT resulted in growth control of multiple MC38-luc tumors. Twelve of 15 (80%) treated mice (Fig. 6G) completely rejected all four tumors, resulting in enhanced survival compared to control (Fig. 6H). Thus, treatment of a single focus of tumor with local NIR-PIT plus systemic PD-1 ICB is sufficient to induce systemic immunity capable of eliminating multiple sites of distant disease not treated with NIR-PIT.

## Development of immunologic memory after combination NIR-PIT and PD-1 ICB

To assess for the presence of immunologic memory, mice were treated with NIR-PIT and PD-1 mAb as before (Supplementary Fig. S9A). Mice that demonstrated a complete response to combination treatment were challenged 30 days later with injection of MC38-luc cells in the contralateral flank (Supplementary Fig. S9B). Whereas control mice readily were engrafted with MC38-luc tumors, mice that previously rejected established MC38-luc tumors resisted engraftment and did not grow tumors (Supplementary Fig. S9C, survival in Supplementary Fig. S9D), demonstrating the presence of immunologic memory.

As depicted in Fig. 7, this and previous work has demonstrated that NIR-PIT induces CD44-specific tumor cell death, leading to the release of multiple tumor antigens. NIR-PIT also promotes a pro-inflammatory tumor microenvironment, resulting in cross priming of multiple antigens and the development of a polyclonal antigen-specific T-cell response. This effector response is limited by PD-1/PD-L1 expression and adaptive immune resistance, which is effectively reversed with the addition of PD-1 ICB.

## Discussion

This and other work has demonstrated on-target cytolytic effects of NIR-PIT monotherapy (1–6), as well as the ability of NIR-PIT to induce immunogenic cell death capable of inducing dendritic cell maturation (7). Batf3$^{+}$ DCs are required for production of chemokine signals that drive trafficking of effector T cells into tumors (23), and type I interferon production by DCs is required for innate activation of adaptive T-cell immunity (24, 25). Here, we demonstrated that NIR-PIT treatment alone induced tumor cell death in multiple models, yet durable antitumor responses were not consistently achieved as established tumors failed to reject completely after monotherapy despite a wild-type immune background. In mice bearing MC38 colon adenocarcinomas or LLC lung carcinomas, NIR-PIT enhanced tumor accumulation of MHC class II$^{+}$ DCs, indicating that DC priming had occurred. TILs within tumors treated with NIR-PIT expressed more PD-1, consistent with their activation, and both tumor and infiltrating immune cells expressed consistent or greater PD-L1 after NIR-PIT, suggesting that adaptive immune resistance could be limiting antitumor immunity. The addition of PD-1 ICB to CD44 NIR-PIT significantly enhanced tumor control in mice bearing MC38 and LLC tumors and led to the induction of robust antitumor immunity. PD-1 ICB reversed adaptive immune resistance, likely induced by local interferon production following NIR-PIT, resulting in systemic antitumor immunity sufficiently potent to induce complete rejection of multiple established tumors. This work serves as proof-of-concept that PD-1 ICB can be used to enhance antitumor immunity induced by NIR-PIT, which can be formulated to target any number of tumor cell surface antigens.

Seminal work by Schreiber and colleagues demonstrated that PD-1 ICB enhances the activity of TILs targeting neoantigens derived from tumor-specific mutated but expressed genes (tumor-specific antigens, TSAs) (26). We did not identify TSAs, but rather, our work assessed specific TIL responses against a panel of tumor-associated antigens (TAAs) known or suspected to be shared amongst MC38, LLC, and MOC1 and with previously identified MHC class I-restricted epitopes (20–22). We demonstrated enhanced TIL responses following NIR-PIT against antigens not targeted at baseline. Not to be confused with the concept of “antigen spread”, which refers to a polyclonal T-cell response following induction of T-cell immunity against a specific antigen with approaches such as peptide vaccination (16, 27), our work demonstrated the ability of NIR-PIT to induce release of multiple TAAs that were processed by DCs leading to a polyclonal T-cell immune response. This work definitively demonstrates the development of polyclonal T-cell responses following tumor-targeting cytolytic therapy. Dovedi et al. demonstrated the ability of IR to increase accumulation of TILs derived from pre-existing T-cell clones based upon sequencing of the TCR repertoire (28). Why NIR-PIT but not other cytotoxic treatment is able to induce a polyclonal T-cell response remains unclear, but may lie with the ability of NIR-PIT to concurrently induce DC maturation through induction of ICD.

Evidence of *de novo* antigen-specific T-cell responses against new antigens following PD-1 ICB is lacking (29). Our data demonstrated enhancement of pre-existing TAA-specific TIL responses following treatment with PD-1 mAb alone, supporting that ICB enhances the antitumor activity of pre-existing but dysfunctional antigen-specific TILs. However, PD-1

ICB enhanced *de novo* TAA-specific TIL responses induced following NIR-PIT as well. Assessment of distant, untreated tumors demonstrated infiltration and activation of TILs that were induced in the treated tumor with combination NIR-PIT and PD-1 ICB, definitively demonstrating the development of systemic antigen-specific antitumor immunity. This has clinical implications for the metastatic disease setting, where if feasible, treatment of one or more sites of disease with tumor-targeting NIR-PIT along with systemic PD-1 ICB could result in systemic antitumor immune responses in lesions not treated with NIR-PIT - analogous to the so called “abscopal effect” infrequently observed with ionizing radiation (30, 31).

As a proof-of-concept study, we targeted CD44 to induce cytolysis. Targeting the CD44 cell surface antigen with NIR-PIT may have multiple benefits. The tumor lines used in this study all expressed high CD44 *in vitro*, but tumor cell CD44 expression *in vivo* was much more heterogeneous between models. CD44 is expressed on tumor cells to a degree in most tumors (32, 33) and can serve as a tumor cell stemness marker (34–36), suggesting that targeting these cells with NIR-PIT may eliminate the cells most resistant to other anti-cancer treatments. However, CD44 is also expressed on activated immune cells within the tumor treatment field, raising the concern that CD44-targeting NIR-PIT could eliminate desirable effector immune cells. Despite this, significant antitumor immunity was induced with combination CD44-targeting NIR-PIT and anti–PD-1. Although not captured in our immune analyses at day 10 after the start of treatment, one possible explanation is that 1–2 NIR-PIT treatments targeting an antigen expressed on tumor-infiltrating immune cells “resets” the immunosuppressive immune microenvironment by eliminating immunosuppressive subsets, similar to induction chemotherapy before adoptive cell transfer immunotherapy (37). Tumor-associated macrophages, MDSCs, and $T_{regs}$ expressed high CD44. IR700 conjugated to an EGFR-targeting antibody is currently in clinical development (RM-1929, NCT02422979). Although EGFR-targeting antibodies are FDA-approved, providing a significant clinical development advantage, it remains to be seen whether NIR-PIT targeting tumor cells alone (with EGFR, for example) will have the same immunostimulatory effects as NIR-PIT targeting more broadly expressed surface antigens.

Several possibilities exist to explain why we did not observe a significant combinatorial effect in MOC1 tumors. First, CD44 tumor cell-specific expression was significantly lower on MOC1 cells *in vivo* compared to LLC or MC38, suggesting that antigen expression is important for the cytolytic effect of NIR-PIT. Next, baseline expression of survivin, Twist1, and Trp53 TAAs was low within MOC1 tumors relative to LLC and MC38. Accordingly, TIL responses against these antigens were not induced following NIR-PIT treatment of MOC1 tumors as they were in LLC and MC38. There was no increase in tumor MHC class $II^+$ DCs or lymphocyte infiltration following NIR-PIT treatment of MOC1 tumors as there was in LLC and MC38, indicating a lack of DC priming. These results suggest that assessment of basic tumor inflammatory responses after NIR-PIT, namely tumor DC and lymphocyte infiltration, could serve as biomarkers of response and select patients most likely to respond to the addition of PD-1 ICB.

Limitations of this study include our inability to replicate the IR700 conjugate currently in clinical development that targets cell surface EGFR (NCT02422979). Multiple attempts to

generate an antibody with high specificity for mouse EGFR were unsuccessful. Given our previous work targeting CD44 with NIR-PIT, we used this cytolytic approach for proof-of-concept studies on antigen release and the development of polyclonal T-cell responses described here. It is possible that using PIT-NIR to target other surface antigens could variably alter T-cell priming, especially if NIR-PIT targeting of $CD44^+$ immunosuppressive immune cell subsets contributes to immune activation. This requires further study.

In conclusion, we have demonstrated the ability of tumor-targeting NIR-PIT to induce tumor cell death and innate priming of polyclonal, antigen-specific T-cell responses in models of colon and lung cancer. These polyclonal responses were enhanced via reversal of adaptive immune resistance with PD-1 ICB, leading to durable antitumor immunity, eradication of both treated and distant untreated tumors, and formation of immunologic memory. These results provide a strong pre-clinical rationale for the treatment of patients with locoregionally advanced or metastatic malignancies with combination NIR-PIT and PD-1 ICB in the trial setting.

## Supplementary Material

Refer to Web version on PubMed Central for supplementary material.

## Acknowledgments

**Funding:** This research was supported by the Intramural Research Program of the National Institutes of Health, National Cancer Institute, Center for Cancer Research (ZIA BC011513) and National Institutes on Deafness and Other Communication Disorders (ZIA DC000087).

## References

1. Mitsunaga M, Ogawa M, Kosaka N, Rosenblum LT, Choyke PL, Kobayashi H. Cancer cell-selective in vivo near infrared photoimmunotherapy targeting specific membrane molecules. Nat Med. 2011; 17: 1685–91. [PubMed: 22057348]
2. Nagaya T, Nakamura Y, Okuyama S, et al. Syngeneic Mouse Models of Oral Cancer Are Effectively Targeted by Anti-CD44-Based NIR-PIT. Mol Cancer Res. 2017; 15: 1667–77. [PubMed: 28923838]
3. Nagaya T, Nakamura Y, Okuyama S, et al. Near-Infrared Photoimmunotherapy Targeting Prostate Cancer with Prostate-Specific Membrane Antigen (PSMA) Antibody. Mol Cancer Res. 2017; 15: 1153–62. [PubMed: 28588059]
4. Nagaya T, Nakamura Y, Sato K, et al. Near infrared photoimmunotherapy with avelumab, an anti-programmed death-ligand 1 (PD-L1) antibody. Oncotarget. 2017; 8: 8807–17. [PubMed: 27716622]
5. Nagaya T, Nakamura Y, Sato K, Harada T, Choyke PL, Kobayashi H. Near infrared photoimmunotherapy of B-cell lymphoma. Mol Oncol. 2016; 10: 1404–14. [PubMed: 27511870]
6. Nagaya T, Nakamura Y, Sato K, et al. Near infrared photoimmunotherapy with an anti-mesothelin antibody. Oncotarget. 2016; 7: 23361–9. [PubMed: 26981775]
7. Ogawa M, Tomita Y, Nakamura Y, et al. Immunogenic cancer cell death selectively induced by near infrared photoimmunotherapy initiates host tumor immunity. Oncotarget. 2017; 8: 10425–36. [PubMed: 28060726]
8. Kepp O, Senovilla L, Vitale I, et al. Consensus guidelines for the detection of immunogenic cell death. Oncoimmunology. 2014; 3: e955691.
9. Freeman GJ, Long AJ, Iwai Y, et al. Engagement of the PD-1 immunoinhibitory receptor by a novel B7 family member leads to negative regulation of lymphocyte activation. J Exp Med. 2000; 192: 1027–34. [PubMed: 11015443]

10. Taube JM, Klein A, Brahmer JR, et al. Association of PD-1, PD-1 ligands, and other features of the tumor immune microenvironment with response to anti-PD-1 therapy. Clinical cancer research : an official journal of the American Association for Cancer Res. 2014; 20: 5064–74.
11. Tumeh PC, Harview CL, Yearley JH, et al. PD-1 blockade induces responses by inhibiting adaptive immune resistance. Nature. 2014; 515: 568–71. [PubMed: 25428505]
12. Ferris RL, Blumenschein G Jr., Fayette J, et al. Nivolumab for Recurrent Squamous-Cell Carcinoma of the Head and Neck. N Engl J Med. 2016; 375: 1856–67. [PubMed: 27718784]
13. Seiwert TY, Burtness B, Mehra R, et al. Safety and clinical activity of pembrolizumab for treatment of recurrent or metastatic squamous cell carcinoma of the head and neck (KEYNOTE-012): an open-label, multicentre, phase 1b trial. Lancet Oncol. 2016; 17: 956–65. [PubMed: 27247226]
14. Chen PL, Roh W, Reuben A, et al. Analysis of Immune Signatures in Longitudinal Tumor Samples Yields Insight into Biomarkers of Response and Mechanisms of Resistance to Immune Checkpoint Blockade. Cancer Discov. 2016; 6: 827–37. [PubMed: 27301722]
15. Farsaci B, Donahue RN, Coplin MA, et al. Immune consequences of decreasing tumor vasculature with antiangiogenic tyrosine kinase inhibitors in combination with therapeutic vaccines. Cancer Immunol Res. 2014; 2: 1090–102. [PubMed: 25092771]
16. Hodge JW, Sharp HJ, Gameiro SR. Abscopal regression of antigen disparate tumors by antigen cascade after systemic tumor vaccination in combination with local tumor radiation. Cancer Biother Radiopharm. 2012; 27: 12–22. [PubMed: 22283603]
17. Judd NP, Winkler AE, Murillo-Sauca O, et al. ERK1/2 regulation of CD44 modulates oral cancer aggressiveness. Cancer Res. 2012; 72: 365–74. [PubMed: 22086849]
18. Feng Z, Jensen SM. Multispectral Imaging of T and B Cells in Murine Spleen and Tumor. 2016; 196: 3943–50.
19. Moore E, Clavijo PE, Davis R, et al. Established T Cell-Inflamed Tumors Rejected after Adaptive Resistance Was Reversed by Combination STING Activation and PD-1 Pathway Blockade. Cancer Immunol Res. 2016; 4: 1061–71. [PubMed: 27821498]
20. Gameiro SR, Higgins JP, Dreher MR, et al. Combination therapy with local radiofrequency ablation and systemic vaccine enhances antitumor immunity and mediates local and distal tumor regression. PLoS One. 2013; 8: e70417.
21. Ciesielski MJ, Kozbor D, Castanaro CA, Barone TA, Fenstermaker RA. Therapeutic effect of a T helper cell supported CTL response induced by a survivin peptide vaccine against murine cerebral glioma. Cancer Immunol Immunother. 2008; 57: 1827–35. [PubMed: 18438666]
22. Hilburger Ryan M, Abrams SI. Characterization of CD8+ cytotoxic T lymphocyte/tumor cell interactions reflecting recognition of an endogenously expressed murine wild-type p53 determinant. Cancer Immunol Immunother. 2001; 49: 603–12. [PubMed: 11225991]
23. Spranger S, Dai D, Horton B, Gajewski TF. Tumor-Residing Batf3 Dendritic Cells Are Required for Effector T Cell Trafficking and Adoptive T Cell Therapy. Cancer Cell. 2017; 31: 711–23 e4. [PubMed: 28486109]
24. Diamond MS, Kinder M, Matsushita H, et al. Type I interferon is selectively required by dendritic cells for immune rejection of tumors. J Exp Med. 2011; 208: 1989–2003. [PubMed: 21930769]
25. Fuertes MB, Kacha AK, Kline J, et al. Host type I IFN signals are required for antitumor CD8+ T cell responses through CD8{alpha}+ dendritic cells. J Exp Med. 2011; 208: 2005–16. [PubMed: 21930765]
26. Gubin MM, Zhang X, Schuster H, et al. Checkpoint blockade cancer immunotherapy targets tumour-specific mutant antigens. Nature. 2014; 515: 577–81. [PubMed: 25428507]
27. Gulley JL, Madan RA, Pachynski R, et al. Role of Antigen Spread and Distinctive Characteristics of Immunotherapy in Cancer Treatment. J Natl Cancer Inst. 2017; 109.
28. Dovedi SJ, Cheadle EJ, Popple AL, et al. Fractionated Radiation Therapy Stimulates Antitumor Immunity Mediated by Both Resident and Infiltrating Polyclonal T-cell Populations when Combined with PD-1 Blockade. Clin Cancer Res. 2017; 23: 5514–26. [PubMed: 28533222]
29. Zappasodi R, Merghoub T, Wolchok JD. Emerging Concepts for Immune Checkpoint Blockade-Based Combination Therapies. Cancer Cell. 2018; 33: 581–98. [PubMed: 29634946]

30. Morisada M, Clavijo PE, Moore E, et al. PD-1 blockade reverses adaptive immune resistance induced by high-dose hypofractionated but not low-dose daily fractionated radiation. Oncoimmunology. 2018; 7: e1395996.

31. Park SS, Dong H, Liu X, et al. PD-1 Restrains Radiotherapy-Induced Abscopal Effect. Cancer Immunol Res. 2015; 3: 610–9. [PubMed: 25701325]

32. Zoller M. CD44: can a cancer-initiating cell profit from an abundantly expressed molecule? Nat Rev Cancer. 2011; 11: 254–67. [PubMed: 21390059]

33. Senbanjo LT, Chellaiah MA. CD44: A Multifunctional Cell Surface Adhesion Receptor Is a Regulator of Progression and Metastasis of Cancer Cells. Front Cell Dev Biol. 2017; 5: 18. [PubMed: 28326306]

34. Jamieson CH, Ailles LE, Dylla SJ, et al. Granulocyte-macrophage progenitors as candidate leukemic stem cells in blast-crisis CML. N Engl J Med. 2004; 351: 657–67. [PubMed: 15306667]

35. Prince ME, Ailles LE. Cancer stem cells in head and neck squamous cell cancer. J Clin Oncol. 2008; 26: 2871–5. [PubMed: 18539966]

36. Singh SK, Clarke ID, Terasaki M, et al. Identification of a cancer stem cell in human brain tumors. Cancer Res. 2003; 63: 5821–8. [PubMed: 14522905]

37. Klebanoff CA, Khong HT, Antony PA, Palmer DC, Restifo NP. Sinks, suppressors and antigen presenters: how lymphodepletion enhances T cell-mediated tumor immunotherapy. Trends Immunol. 2005; 26: 111–7. [PubMed: 15668127]

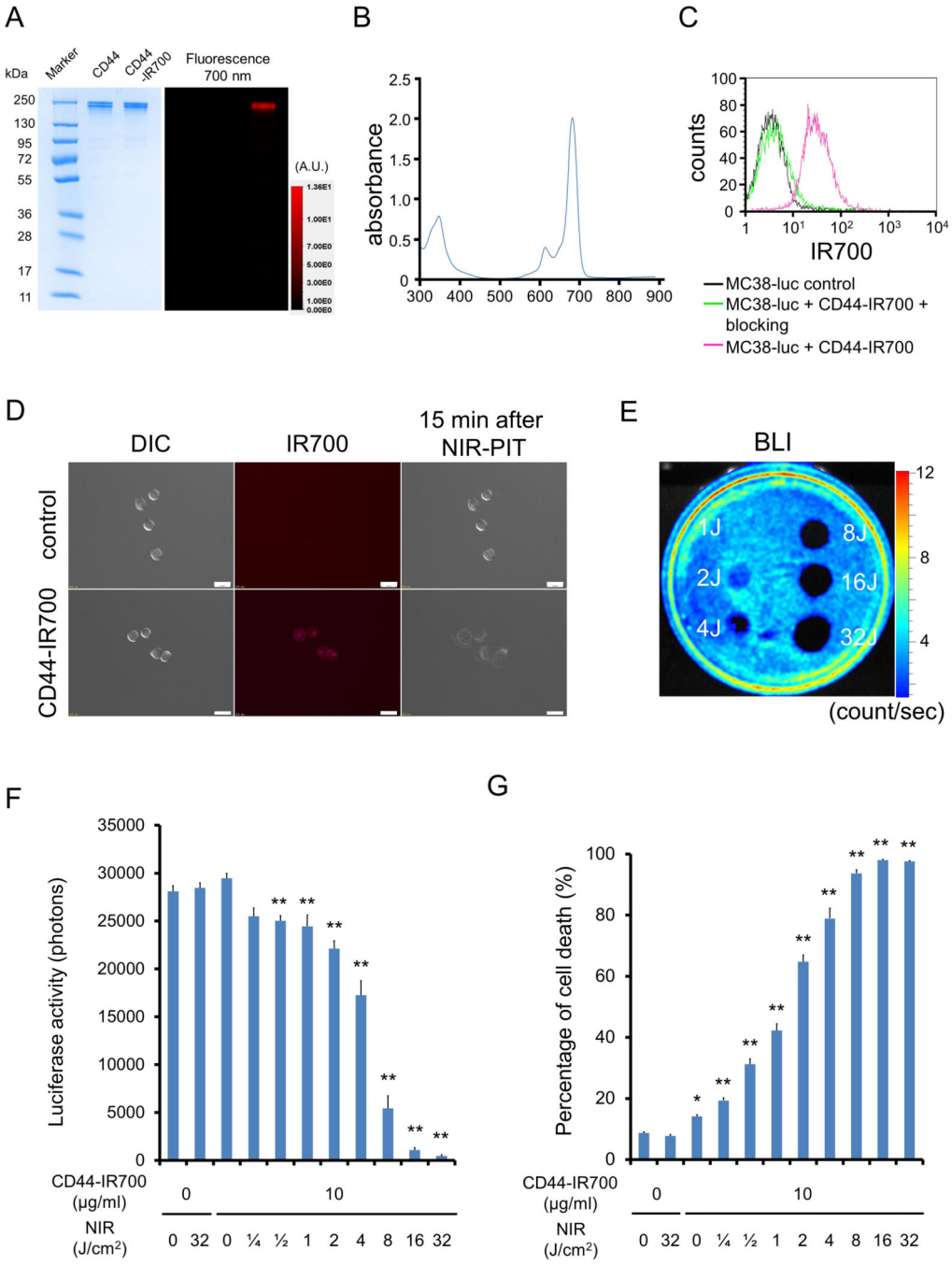


**Figure 1. Confirmation of CD44 expression as a target for NIR-PIT in MC38-luc cells and evaluation of *in vitro* NIR-PIT.**

(A) Validation of CD44-IR700 by SDS-PAGE (left: Colloidal Blue staining; right: IR700 fluorescence). Diluted anti-CD44 was used as a control. (B) Absorbance curve of CD44-IR700. (C) Expression of cell surface CD44 in MC38-luc cells was examined with flow cytometry. CD44-blocking antibody was added to some wells to validate specific staining. Representative histograms shown. (D) Differential interference contrast (DIC) and fluorescence microscopy images of MC38-luc cells. Change in MC38-luc cellular architecture following 15 minutes of NIR light exposure shown. Scale bars = 20 μm. (E)

Bioluminescence imaging (BLI) demonstrating luciferase activity in MC38-luc cells following NIR-light. (F) Quantification of MC38-luc luciferase activity after labelling with CD44-IR700 and treatment with NIR-light (n = 5, $^{**}p < 0.01$ vs. untreated control, Student's t test). (G) Membrane permeability of MC38-luc cells, as measured by propidium iodide (PI) staining, after labeling with CD44-IR700 and treatment with NIR-light (n = 5, $^{*}p < 0.05$ vs. untreated control, $^{**}p < 0.01$ vs. untreated control, Student's t test). Each value represents mean ± standard error of the mean (SEM) of five independent experiments.

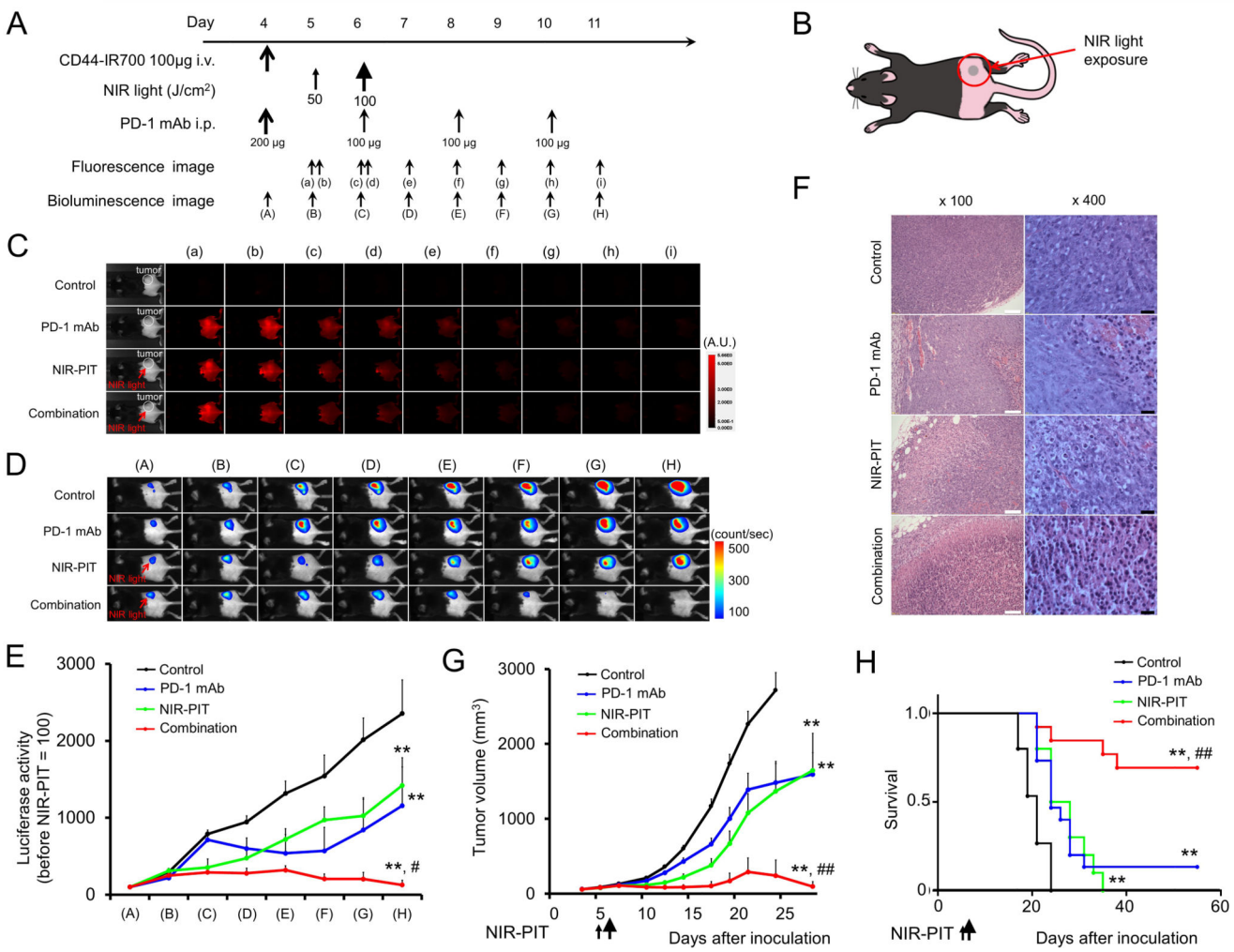


**Figure 2. *In vivo* effect of NIR-PIT and PD-1 mAb in mice bearing a unilateral MC38-luc tumors.**

(A) NIR-PIT regimen. Bioluminescence and fluorescence images were obtained at each time point as indicated. (B) Light exposure. NIR light was administered to the unilateral right-sided tumor. (C) *In vivo* IR700 fluorescence real-time imaging of tumor-bearing mice in response to NIR-PIT (n=10). (D) *In vivo* BLI of tumor bearing mice in response to NIR-PIT. Mice in the PD-1 mAb group also received CD44-IR700 but were not treated with NIR. (E) Quantification of luciferase activity in four treatment groups (n ≧ 10, $^{**}p < 0.01$ vs. control, Tukey's t test with ANOVA; $^{\#}p < 0.05$ vs. PD-1 mAb and NIR-PIT groups, Tukey's t test with ANOVA). (F) Resected tumors (day 10) were stained with H&E and assessed for necrosis and leukocyte infiltration. White scale bars = 100 μm. Black scale bars = 20 μm. (G) Tumor growth curves (n ≧ 10, $^{**}p < 0.01$ vs control, Tukey's t test with ANOVA; $^{\#\#}p < 0.01$ vs PD-1 mAb and NIR-PIT groups, Tukey's t test with ANOVA). (H) Kaplan-Meier survival analysis following NIR-PIT treatment with and without PD-1 mAb ($^{**}p < 0.01$ vs. control, Log rank test; $^{\#\#}p < 0.01$ vs. PD-1 mAb and NIR-PIT groups, Log rank test).

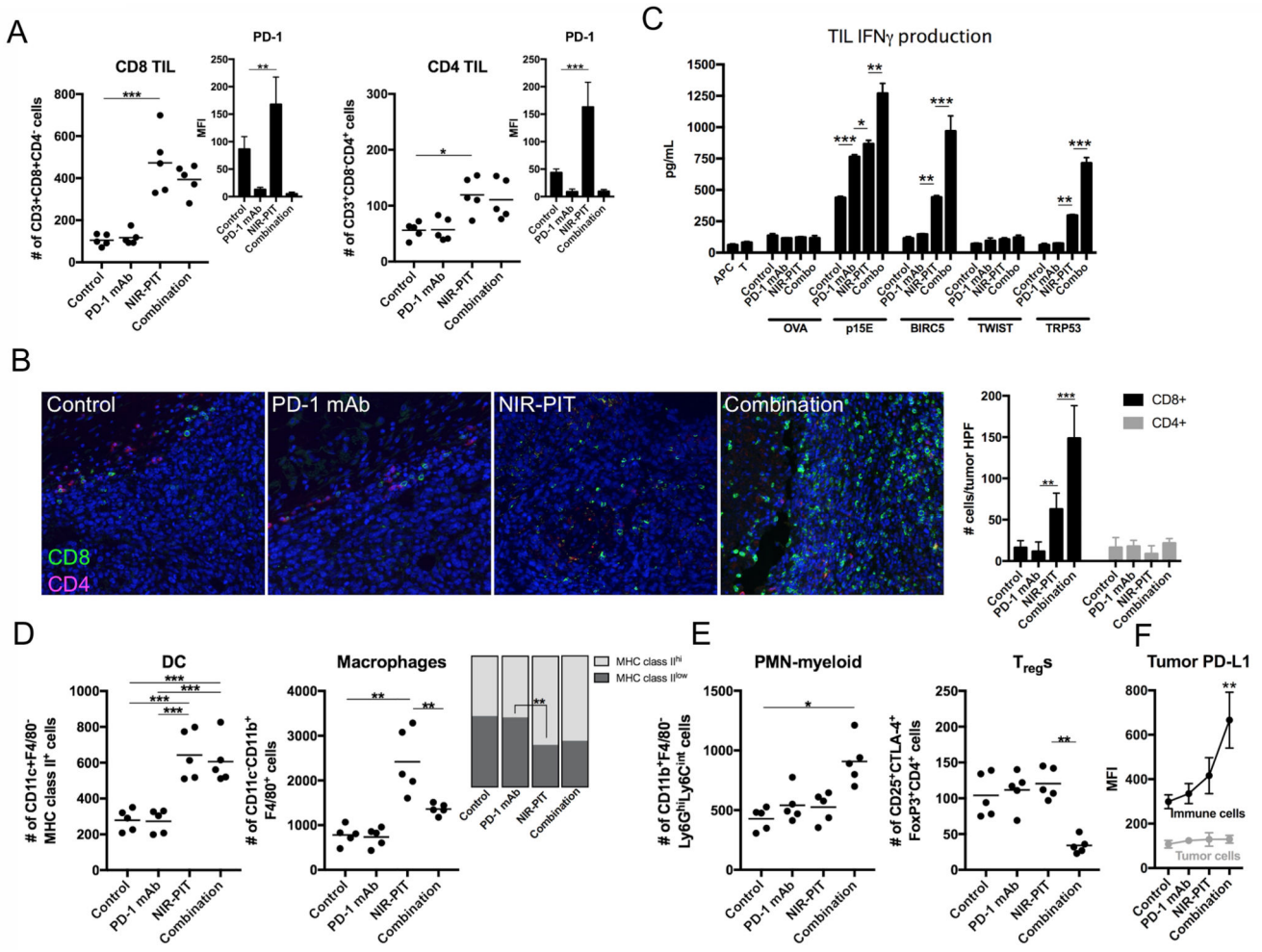


**Figure 3. Immune correlative and functional effects of NIR-PIT and PD-1 mAb in mice bearing a unilateral MC38-luc tumors.**

(A) MC38-luc tumors (day 10, n = 5/group) treated with NIR-PIT with and without PD-1 mAb and controls were harvested, digested into single-cell suspensions, and analyzed for tumor-infiltrating lymphocytes (TILs) via flow cytometry. Presented as absolute number of infiltrating cells per $1.5 \times 10^4$ live cells analyzed. PD-1 expression shown as inset (MFI, mean fluorescence intensity). *$p < 0.05$, **$p < 0.01$, ***$p < 0.001$, t test with ANOVA. Representative data from one of two independent expeirments shown. (B) Multiplex immunofluorescence was used to validate flow cytometric data. Representative 400× images shown. Quantification of infiltrating TILs from 5 high power fields (HPF) per tumor, n = 3/group. **$p < 0.01$, ***$p < 0.001$, t test with ANOVA. (C) TILs were isolated from tumors treated as above (n = 5/group) via an IL2 gradient, enriched via negative magnetic selection, and stimulated with irradiated splenocytes pulsed with peptides representing known MHC class I-restricted epitopes from selected tumor-associated antigens. IFNγ production was determined by ELISA from supernatants collected 24 hours after stimulation. Supernatants from splenocytes (APCs) alone, TILs (T) alone, and a MHC-class I-restricted epitope from ovalbumin (OVA, SIINFEKL) were used as controls. *$p < 0.05$, **$p < 0.01$, ***$p < 0.001$, t test with ANOVA. (D) Flow cytometric analysis of tumor-infiltrating DCs and macrophages,

with quantification of macrophage polarization based on MHC class II expression. $^{**}p < 0.01$, $^{***}p < 0.001$, t test with ANOVA. (E) Flow cytometric analysis of tumor infiltrating neutrophilic myeloid cells (PMN-myeloid) and regulatory T-cells ($T_{regs}$). $^{*}p < 0.05$, $^{**}p < 0.01$, t test with ANOVA. (F) Flow cytometric analysis of PD-L1 expression on $CD45.2^{-}CD31^{-}PDGFR^{-}$ tumor cells and $CD45.2^{+}CD31^{-}$ immune cells. $^{**}p < 0.01$ compared to control, t test with ANOVA. N = 5/group.

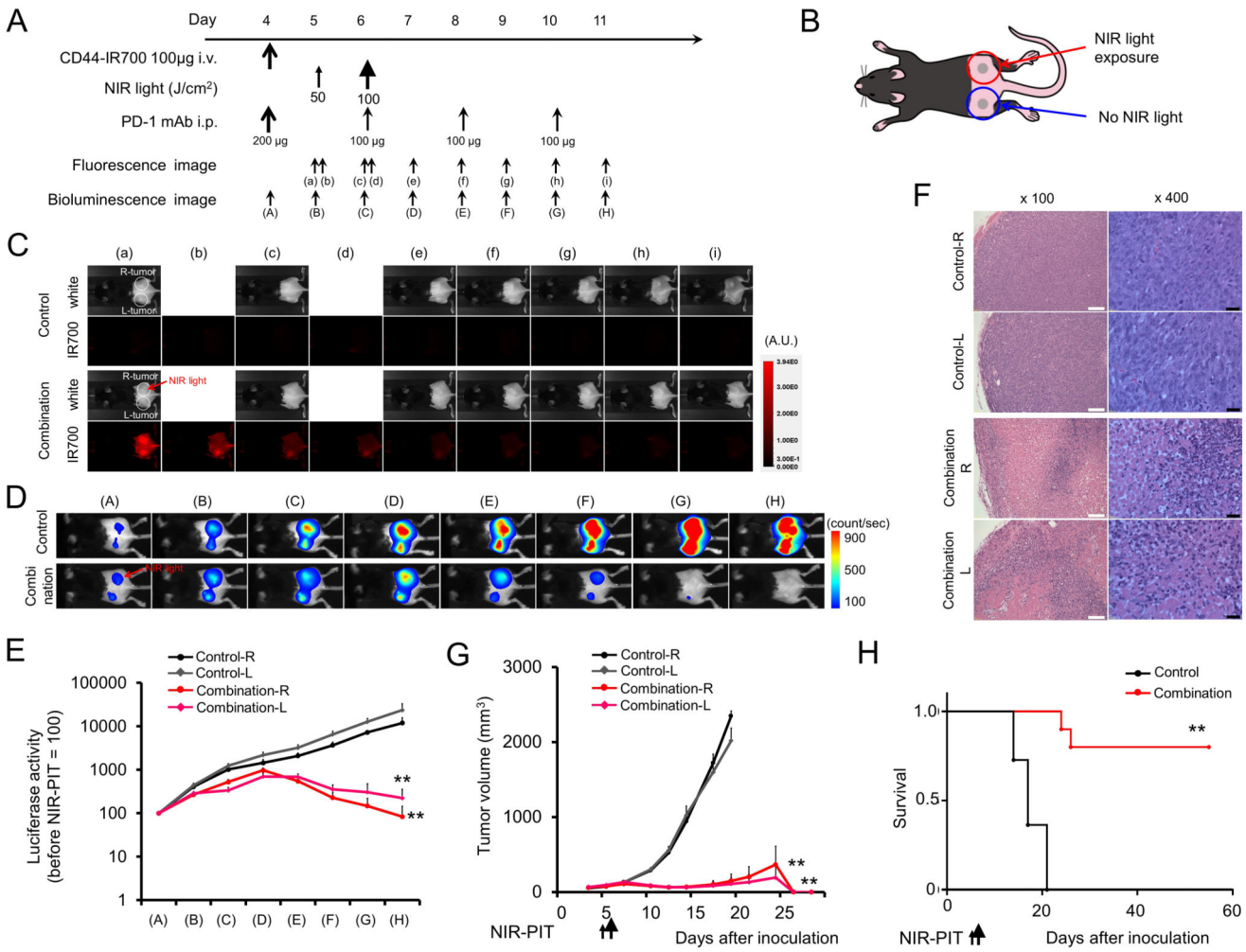


**Figure 4. *In vivo* effect of NIR-PIT and PD-1 mAb in mice bearing bilateral MC38-luc tumors.**

(A) NIR-PIT regimen. Bioluminescence and fluorescence images were obtained at each time point as indicated. (B) Light exposure. NIR light was administered to the right-side tumor only in mice bearing bilateral lower flank tumors. The untreated left-side tumor was shielded from NIR light. (C) *In vivo* IR700 fluorescence real-time imaging of tumor-bearing mice in response to NIR-PIT to the right-side tumor only. (D) *In vivo* BLI of tumor bearing mice in response to combination NIR-PIT and PD-1 mAb. (E) Quantification of luciferase activity from each tumor in controls and mice treated with combination NIR-PIT and PD-1 mAb (n = 10, $^{**}p < 0.01$, Tukey's test with ANOVA). (F) Resected tumors (day 10) were stained with H&E and assessed for necrosis and leukocyte infiltration. White scale bars = 100 μm. Black scale bars = 20 μm. (G) Growth curves of right- and left-side tumors from controls and mice treated with combination NIR-PIT and PD-1 mAb. (H) Kaplan-Meier survival analysis from controls and mice treated with combination NIR-PIT and PD-1 mAb (n = 10, $^{**}p < 0.01$, Tukey's test with ANOVA for growth curves; $^{**}p < 0.01$, Log-rank test for survival).

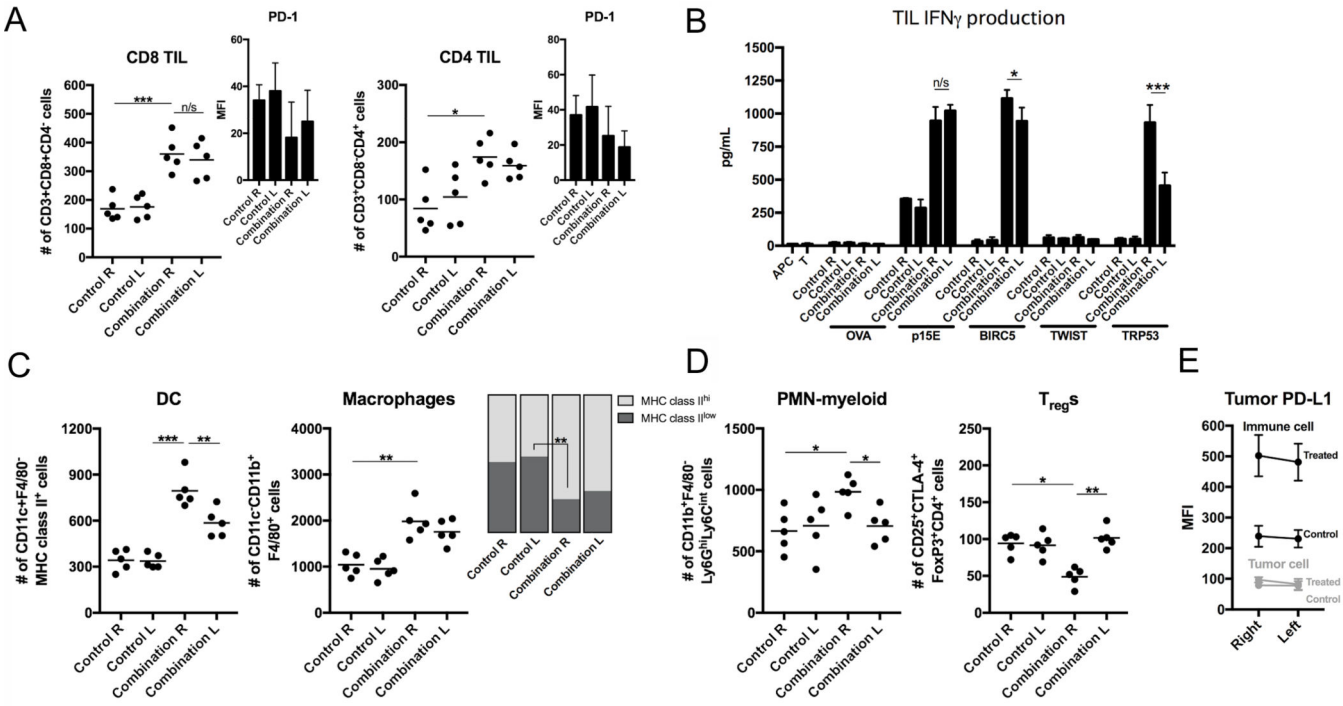


**Figure 5. Immune correlative and functional effects of NIR-PIT and PD-1 mAb in mice bearing a bilateral MC38-luc tumors.**

(A) Bilateral MC38-luc tumors (day 10, n = 5/group) treated with PD-1 mAb with or without NIR-PIT and bilateral control tumors were harvested, digested into single-cell suspensions, and analyzed for tumor-infiltrating lymphocytes (TILs) via flow cytometry. Presented as absolute number of infiltrating cells per $1.5 \times 10^4$ live cells analyzed. PD-1 expression shown as inset (MFI, mean fluorescence intensity). $*p < 0.05$, $***p < 0.001$, t test with ANOVA. Representative data from one of two independent expeirments shown. (B) TILs were extracted from tumors treated as above (n = 5/group) via an IL2 gradient, enriched via negative magnetic selection, and stimulated with irradiated splenocytes pulsed with peptides representing known MHC class I-restricted epitopes from selected tumor-associated antigens. IFNγ production was determined by ELISA from supernatants collected 24 hours after stimulation. Supernatants from splenocytes (APC) alone, TILs (T) alone, and a MHC-class I-restricted epitope from ovalbumin (OVA, SIINFEKL) were used as controls. $*p < 0.05$, $***p < 0.001$, t test with ANOVA. (C) Flow cytometric analysis of tumor-infiltrating DCs and macrophages, with quantification of macrophage polarization based on MHC class II expression. $**p < 0.01$, $***p < 0.001$, t test with ANOVA. (D) Flow cytometric analysis of tumor-infiltrating PMN-myeloid and $T_{regs}$. $*p < 0.05$, $**p < 0.01$, t test with ANOVA. (E) Flow cytometric analysis of PD-L1 expression on $CD45.2^{-}CD31^{-}$ $PDGFR^{-}$ tumor cells. N = 5/group.

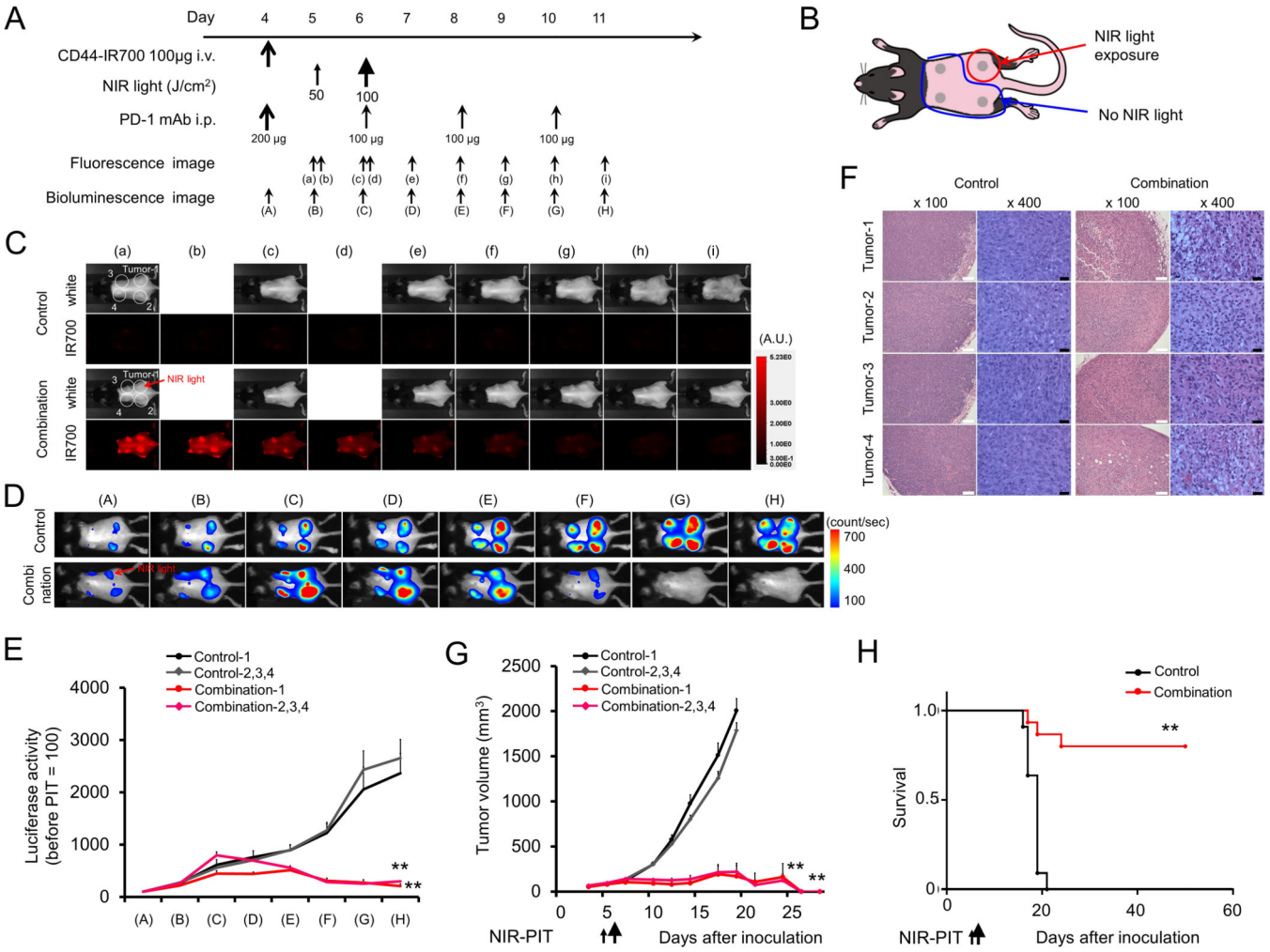


**Figure 6. *In vivo* effect of NIR-PIT and PD-1 mAb in mice bearing multiple MC38-luc tumors.**

(A) NIR-PIT regimen. Bioluminescence and fluorescence images were obtained at each time point as indicated. (B) Light exposure. NIR light was administered to the caudal right-side tumor only in mice bearing four tumors. All other tumors were shielded from NIR light. (C) *In vivo* IR700 fluorescence real-time imaging of tumor-bearing mice in response to NIR-PIT treatment to the caudal right-side tumor only. (D) *In vivo* BLI of tumor bearing mice in response to NIR-PIT treatment of the caudal right-side tumor only. (E) Quantification of luciferase activity in all tumors from controls and mice treated with combination NIR-PIT and PD-1 mAb. Only the caudal right-side tumor received NIR-PIT treatment (n = 10, $^{**}p < 0.01$, Tukey's test with ANOVA). (F) Resected tumors (day 10) were stained with H&E and assessed for necrosis and leukocyte infiltration. White scale bars = 100 μm. Black scale bars = 20 μm. (G) Growth curves from controls and treated and untreated tumors from mice receiving combination NIR-PIT and PD-1 mAb. (H) Kaplan-Meier survival analysis (n = 10, $^{**}p < 0.01$, Tukey's test with ANOVA for growth curves; $^{**}p < 0.01$, Log-rank test for survival).

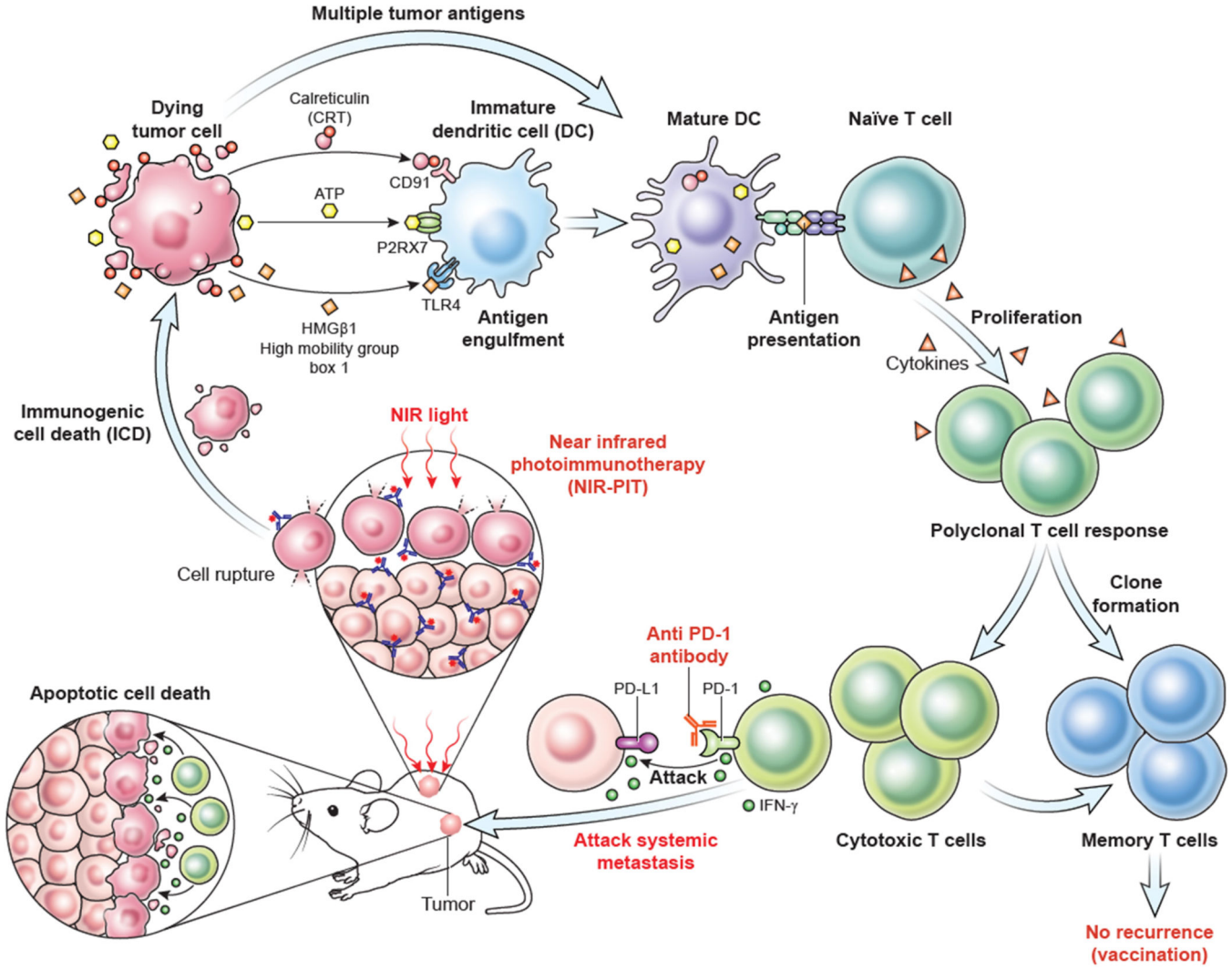


**Figure 7. Proposed mechanism of combination treatment with local NIR-PIT and systemic PD-1 mAb.**

Following NIR-PIT cellular damage, tumor cells undergo immunogenic cell death (ICD) with release of innate immune ligands, such as calreticulin (CRT), ATP, and high mobility group box 1 (HMGB1), along with multiple tumor antigens. Following processing and presentation of these antigens by matured antigen-presenting cells such as DCs, a systemic polyclonal T-cell response develops. However, PD-1 expression on activated T-cells and PD-L1 expression within the tumor microenvironment leads to adaptive immune resistance and dysfunctional T-cells. PD-1 immune checkpoint blockade reverses this adaptive immune resistance, resulting in activation of TILs specific for multiple tumor antigens at both primary and distant (abscopal) sites of disease, complete tumor rejection, and immunologic memory.